Electrocatalysis for the Hydrogen Economy

Ioannis Katsounaros and Marc T.M. Koper

Abstract This chapter deals with the concept of "hydrogen economy", which was introduced by John O.M' Bockris in 1972. We summarize the fundamental principles and the progress for the reactions relevant to the hydrogen economy, namely the hydrogen and oxygen evolution for water electrolyzers, and the hydrogen oxidation and oxygen reduction for fuel cells. The activity of each reaction can be correlated to a single descriptor, i.e. the adsorption energy of a key reaction intermediate, following a volcano-type relationship. Highly active materials can be prepared with the aid of modern computational and experimental tools. Nevertheless, to develop catalysts that are substantially more active and reach the performance of ideal catalysts, the focus must be placed on materials that can break the energetic scaling relations between intermediates. The systems of choice are acidic water electrolyzers or fuel cells, using noble metals for the catalytic material, despite the great progress made in the field of alkaline systems. However, to realize the concept of hydrogen economy on a large scale, the electrode material for either reaction must combine activity, stability and abundance.

1 Introduction

In Jules Verne's 1874 novel "The mysterious island", the engineer Cyrus Smith explains to his fellow prisoners his belief that "*water will one day be employed as fuel, that hydrogen and oxygen which constitute it, used singly or together,*

I. Katsounaros
Forschungszentrum Jülich GmbH, Helmholtz-Institut Erlangen-Nürnberg (HI ERN),
91058 Erlangen, Germany
e-mail: i.katsounaros@fz-juelich.de

M.T.M. Koper (✉)
Leiden Institute of Chemistry, Leiden University, PO Box 9502,
2300RA Leiden, The Netherlands
e-mail: m.koper@lic.leidenuniv.nl

K. Uosaki (ed.), *Electrochemical Science for a Sustainable Society*,
DOI 10.1007/978-3-319-57310-6_2

will furnish an inexhaustible source of heat and light, of an intensity of which coal is not capable" [1]. One hundred years later, in a letter to *Science*, John O'M. Bockris gave a scientific outlook to these words by introducing the term "hydrogen economy": Bockris' vision for a paradigm shift in meeting the increasing global energy needs with hydrogen acting as the primary energy carrier [2]. Bockris used the term "economy" to emphasize the energetic, economic, ecological and societal aspects of his idea. In brief, this concept was originally based on converting the plentiful and inexpensive electrical energy delivered by nuclear stations to chemical energy, by splitting water and thereby producing hydrogen in onsite water electrolyzers. After transportation to distribution stations and to final locations (houses, factories, vehicles, trains, aircrafts, etc.), the produced hydrogen would be used in an onsite fuel cell to deliver electrical energy. The advantages of Bockris' concept were obvious: the rapidly increasing energy demand would be met at a lower cost without polluting the environment, while the dependence on fossil fuels would become minimal.

When Verne was writing his book, he was probably aware of two independent observations which set the scientific stage for the "hydrogen economy": In 1789, the Dutch Adriaan Paets van Troostwijk and the German-Dutch Johan Rudolph Deiman observed that gas bubbles form on two gold wires immersed in water, when they are connected to an electrostatic generator, and they realized that they had "split" water into hydrogen and oxygen [3]. Fifty years later, in 1839, the British Sir William Grove described in a letter to the *Philosophical Magazine* how he was able to produce electricity by connecting two platinum wires, immersed in an acidic solution through two glass tubes, one filled with hydrogen and one with oxygen [4]. The observation that oxygen and hydrogen can recombine by producing electricity was actually mentioned a few months before Grove's publication, by the German Christian Friedrich Schönbein [5]. In principle, Van Troostwijk and Deiman were the first ones to split water into its components, while Grove and Schönbein had prepared the first, very primitive fuel cell.

The original concept of Bockris in 1972 included the utilization of nuclear energy for supplying the necessary energy to produce H_2 via water splitting and to set the hydrogen economy in motion. In the years that followed, however, a modification of this idea became necessary: the Chernobyl accident in 1986 raised severe concerns for the use of nuclear power, and concomitantly, there was a boost in the interest for the exploitation of renewable energy sources. Therefore, the modern interpretation of the "hydrogen economy" concept involves the utilization of renewable instead of nuclear energy, as the first step to split water and generate hydrogen. It is evident, however, that the central idea of John Bockris to use hydrogen as the primary means of storing and transporting energy remained unaltered. In fact, the concept of "hydrogen economy" is nowadays at the focus of academic, technological and industrial interest and plays a key role in the research conducted in the fields of electrochemistry, (electro-)chemical engineering, materials science, computational chemistry and others.

The focus in this chapter is the core of the 'hydrogen economy' principle, namely the electrochemical reactions of hydrogen and oxygen evolution for the water electrolyzers, and the hydrogen oxidation and oxygen reduction reaction for the low-temperature hydrogen–air fuel cells. We will (i) demonstrate the fundamental principles that govern the above mentioned reactions, (ii) summarize the important progress that was made in the field over the last decades, and (iii) discuss the future prospects towards the realization of Bockris' and Verne's vision.

2 Water Electrolyzers and Fuel Cells—The Basic Principle

In water electrolysis cells (water electrolyzers) the oxygen evolution reaction (OER) occurs at the anode (positive electrode) and the hydrogen evolution reaction (HER) occurs at the cathode (negative electrode) (see Scheme 1, left). Inversely in a hydrogen–air fuel cell, the hydrogen oxidation reaction (HOR) takes place at the anode (negative electrode) and the oxygen reduction reaction (ORR) occurs at the cathode (positive electrode) (see Scheme 1, right). The overall reaction occurring in a water electrolyzer (forward reaction, left-to-right) or in a hydrogen–oxygen fuel cell (back reaction, right-to-left) is described by (1):

$$2H_2O \rightleftharpoons O_2 + 2H_2. \tag{1}$$

At standard conditions, the Gibbs free energy of the forward non-spontaneous water splitting reaction is +474.4 kJ per 1 mol of O_2 evolved. Thus, water splitting can take place only with the supply of electrical energy, i.e. by applying a potential of at least 1.229 V between the two electrodes. The Gibbs free energy of the reverse spontaneous reaction is equal but of opposite sign.

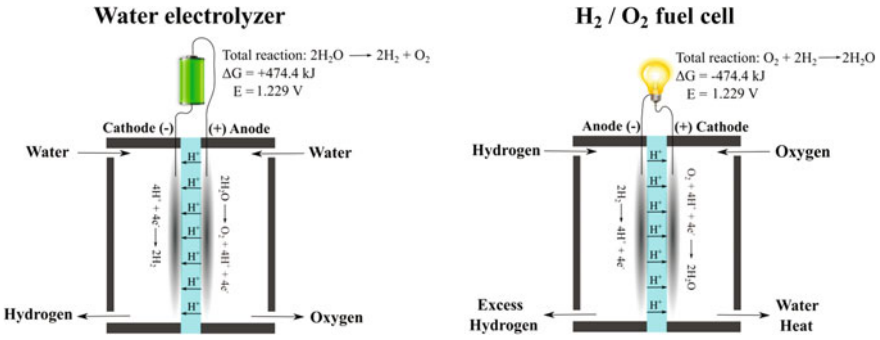

Scheme 1 Principle of operation of water electrolyzers (*left*) and hydrogen–oxygen fuel cells (*right*) under acidic conditions

2.1 Fundamentals of the ORR and the OER

The oxygen reduction and the reverse water oxidation are multi-step processes and involve the transfer of up to four electrons [6]:

$$O_2 + 4H^+ + 4e^- \rightleftarrows 2H_2O \quad E_{O_2/H_2O} = +1.229\,\text{V vs RHE} \tag{2}$$

where E is the standard equilibrium potential of the reaction with respect to the reversible hydrogen reference electrode (RHE). Such multi-electron processes proceed sequentially through the formation of several intermediates. Depending on the followed mechanism, reaction intermediates can be *OOH, *O, *OH, *HOOH or dissolved H_2O_2, where the asterisk denotes adsorbed species. The distinction between the mechanisms is based on the number of proton/electron transfer steps that precede the O–O bond cleavage (for the ORR) or formation (for the OER) [7–9]. The only possible intermediate of the overall reaction (2) that can desorb is hydrogen peroxide [10]:

$$O_2 + 2H^+ + 2e^- \rightleftarrows H_2O_2 \quad E_{O_2/H_2O_2} = +0.695\,\text{V vs RHE} \tag{3}$$

$$H_2O_2 + 2H^+ + 2e^- \rightleftarrows 2H_2O \quad E_{H_2O_2/H_2O} = +1.709\,\text{V vs RHE.} \tag{4}$$

The participation of H_2O_2 in the reaction sequence remains debateable. The standard equilibrium potentials shown in (3) and (4) are calculated for a solution with the standard activity of H_2O_2 equal to one. Thus, in thermodynamic terms it cannot be excluded that a small amount of H_2O_2 forms as an intermediate from the ORR at potentials more positive than +0.695 V_{RHE} or from the OER at potentials less positive than +1.709 V_{RHE} [10]. Indeed, the comparison between the O_2 and H_2O_2 reduction shows that the two reactions follow the same trends in different electrolytes or surfaces (low- and high-index Pt facets), indicating that the ORR is likely to proceed through an H_2O_2-mediated pathway [11–13]. Similar studies on the oxidation of H_2O_2 under conditions relevant to the OER are not known.

The ideal catalyst would carry out both reactions at the reversible potential, i.e. at +1.23 V_{RHE}. This would be achieved only if there was no uphill step during either the ORR or the OER at this potential; namely, if the difference in the free energy of the species involved in each step was zero [14]. Real catalysts, however, deviate from the ideal scenario. Density functional theory (DFT) calculations allow the calculation of the free energies of the species [14] and show that there are three endothermic steps for the ORR, i.e. OOH* formation, *O hydrogenation and *OH desorption (see the black diagram from left-to-right in Fig. 1), while the OER is associated with the strongly endothermic *O + *OH recombination (see black diagram from right-to-left). These calculations are made for Pt(111) at the reversible potential (+1.23 V_{RHE}). To render all steps exothermic for each individual reaction an overpotential is required, i.e. a potential as low as +0.78 V_{RHE} for the ORR and as high as +2.55 V_{RHE} for the OER (Fig. 1). The comparison between the solid and dashed diagrams shows the deviation of free energies for Pt(111) from the ideal

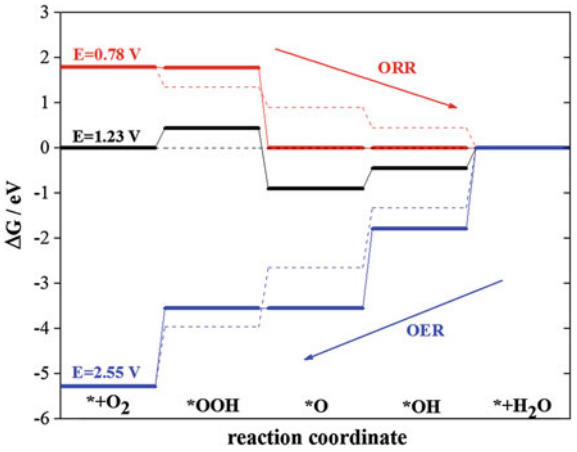

Fig. 1 Free energy diagram for the ORR (*left*-to-*right*) or the OER (*right*-to-*left*) for a bare Pt(111) surface (*solid diagram*) or an ideal catalyst (*dashed diagram*), at the reversible potential (1.23 V), and at a potential for which all steps become exothermic (+0.78 V for the ORR or +2.55 V for the OER). All free energies are expressed with respect to the free energy of liquid water. Reproduced from [14] with permission from Elsevier

catalyst. The description above includes the assumption that the ORR and the OER proceed via the same intermediates, i.e. *OOH, *O and *OH. It must be mentioned, however, that Fig. 1 shows a unified scheme for the ORR and the OER for an oxygen-free Pt(111) surface, and thus it must be assessed only qualitatively because the OER for instance takes place on an oxide-covered surface.

The deviation of real catalysts from the ideal performance is imposed by the scaling relations between the free energies of adsorption of the ORR or OER intermediates that hold for metal surfaces [15, 16]. The free energies of adsorption of *OOH, *O and *OH on (111) surfaces at a given potential, E, are related to each other through the following equations [14]:

$$\left(\Delta G^{E}_{*OOH} + 3 \times E\right) = 0.53 \times \left(\Delta G^{E}_{*O} + 2 \times E\right) + 3.33\,eV \tag{5}$$

$$\left(\Delta G^{E}_{*OH} + 1 \times E\right) = 0.50 \times \left(\Delta G^{E}_{*O} + 2 \times E\right) + 0.04\,eV. \tag{6}$$

The factors multiplied by the potential, E, represent the number of electrons required to form the respective species from water, i.e. 1 for *OH, 2 for *O and 3 for *OOH. Scaling relations also apply for metal oxides with the expressions being slightly different than for (111) metal surfaces [17]:

$$\left(\Delta G^{E}_{*OOH} + 3 \times E\right) = 0.64\left(\Delta G^{E}_{*O} + 2 \times E\right) + 2.40\,eV \tag{7}$$

$$\left(\Delta G^{E}_{*OH} + 1 \times E\right) = 0.61\left(\Delta G^{E}_{*O} + 2 \times E\right) - 0.58\,eV. \tag{8}$$

Therefore, independent of the nature of the metal or metal oxide, the difference $\Delta G_{*OOH} - \Delta G_{*OH}$ will be ca. (3.29 – 2 × E) eV for (111)-metals or (2.98 – 2 × E) eV for metal oxides, which is 0.83 or 0.52 eV higher than what is required for the

ideal catalyst for either the ORR or the OER, respectively. These differences are fixed for all metal or metal oxide surfaces, respectively, as long as (i) the reaction intermediates involved are the same and (ii) adsorbates bind in the same way, i.e. through the same atom. The thermodynamic limitations introduced by scaling relations can in principle be avoided using catalysts that bind the intermediates on different sites, as this would allow tuning the adsorption energy of one adsorbate independently of the other [15].

The scaling relations allow the derivation of standard equilibrium potentials as a function of a single free energy of adsorption, e.g. the ΔG_O:

- For ORR on (111) surfaces, assuming an $O_2 \rightarrow *OOH \rightarrow *O + *OH$ $2*OH \rightarrow H_2O$ pathway:

$$E_{O_2/*OOH} = \frac{1}{e_o} \times (\Delta G_O + 1.59) \tag{9}$$

$$E_{*OOH/*OH} = \frac{1}{e_o} \times (0.03\Delta G_O + 3.29) \tag{10}$$

$$E_{*OH/H_2O} = \frac{1}{e_o} \times (0.50\Delta G_O + 0.04). \tag{11}$$

- For the OER on metal oxides, assuming an $H_2O \rightarrow *OH \rightarrow *O \rightarrow *OOH \rightarrow O_2$ pathway:

$$E_{*OH/H_2O} = \frac{1}{e_o} \times (0.61\Delta G_O - 0.58) \tag{12}$$

$$E_{*O/*OH} = \frac{1}{e_o} \times (0.39\Delta G_O + 0.58) \tag{13}$$

$$E_{*OOH/*O} = \frac{1}{e_o} \times (-0.36\Delta G_O + 2.40) \tag{14}$$

$$E_{O_2/*OOH} = \frac{1}{e_o} \times (-0.64 + 2.52). \tag{15}$$

Thus, the ΔG_{*O} can be used as a single descriptor for the construction of thermodynamic volcano-type plots. For example, Fig. 2 shows the standard equilibrium potentials for the various steps of the ORR or the OER [15]. Note that contrary to Fig. 1 which was drawn for Pt(111) for both reactions, here the volcanoes are constructed for metal (111) and for metal oxide surfaces for the ORR and the OER, respectively. The thick curves in Fig. 2 represent the onset potential for each reaction, and the volcano develops by a change in the

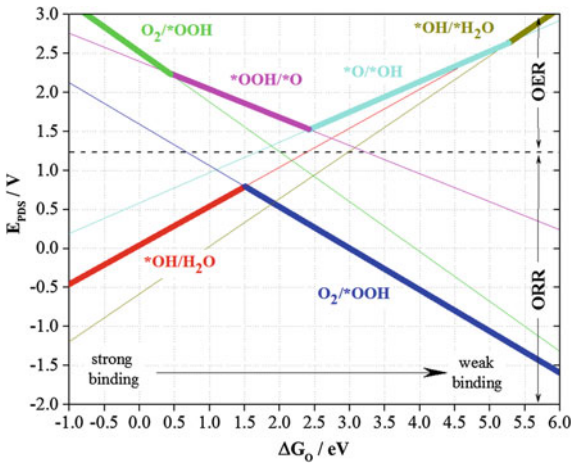

Fig. 2 Thermodynamic volcano plots for the ORR on metal (111) surfaces and for the OER for metal oxides, as derived from the solution of Eqs. (9)–(15). The *thick curves* represent the potential at which the free energy of all steps of the respective reaction is negative. The potential-determining step is denoted in the figure legends. The ORR was assumed to follow the $O_2 \rightarrow$ *OOH $\rightarrow$ *O + *OH $\rightarrow$ 2*OH $\rightarrow$ H_2O pathway, and the OER the $H_2O \rightarrow$ *OH *O $\rightarrow$ *OOH $\rightarrow$ O_2 pathway. The *dashed curve* represents the standard potential for the O_2/H_2O couple. Reproduced from [15] with permission from Elsevier

potential-determining step[1] as the metal–oxygen bond becomes weaker from left to right. For instance, on the left-hand side of the volcano (strong *O binding) the ORR is limited by *OH desorption while on the right-hand side (weak *O binding) the potential-determining step is the formation of *OOH. The optimum catalyst, i.e. at the top of the volcano, achieves a compromise between strong and weak *O binding. For the OER, there are four potential-determining steps depending on the free energy of adsorption for *O, but the most relevant ones near the top of the volcano are the O–O bond formation for strong *O binding (left-hand side) and the *OH dehydrogenation for weak *O binding (right-hand side). For both reactions, the top of the volcano is accompanied with a deviation from the reversible potential, i.e. with an overpotential, which cannot be avoided when a metal or a metal oxide surface is used for the ORR or the OER, respectively, as long as the above scaling relations are satisfied.

The volcano plot in Fig. 2, derived purely based on thermodynamics, is in principle different from an (experimental) volcano plot that has an activity term on the vertical axis and is thus based on kinetics. However, the E_{PDS} is a reliable measure of the overall reaction rate, as long as a relation between the activation

[1]The potential-determining step, E_{PDS}, is the reaction step with the most unfavourable equilibrium potential, i.e. the step that determines at which potential all reaction steps will become exothermic [18].

energy and the reaction energy (Brønsted–Evans–Polanyi principle [19]) applies. Therefore, thermodynamic volcanoes are typically in good, qualitative agreement with kinetic volcanoes.

3 Oxygen Evolution Reaction

The oxygen evolution takes place on oxide surfaces. The oxide may undergo redox transitions depending on the potential, which makes it more complicated to rationalize structure–activity relationships. Trasatti summarized the early efforts to develop activity descriptors for the OER and showed that the experimental OER activity for some rutile- or spinel-type oxides follows a volcano-type relationship, with the descriptor being the standard enthalpy of the lower-to-higher transition [20].

Rutile-type oxides of precious metals have attracted most of the interest in acidic electrolytes, because they are supposed to be more stable toward dissolution compared to oxides of non-noble metals. The activity of precious metal oxides in acid increases in the order Au < Pt < Pd < Rh < Ir < Ru [21]. The same activity trend is also observed for nanoparticulate catalysts [22]. The activities of RuO_2 and IrO_2 are lower in alkaline compared to acid; however, RuO_2 remains the most active material with the IrO_2 following [23]. These activity trends are consistent with the *O binding energy on the metal oxides; for example RuO_2 and IrO_2 bind O with nearly the optimal adsorption energy [24]. One important feature of the OER on noble metal oxide surfaces is that the mechanism of the reaction seems to be different among the oxides. Differential electrochemical mass spectrometry (DEMS) studies using isotope-labelled oxide (^{18}O) at the surface and non-labelled $H_2^{16}O$ for the electrolyte showed that the metal oxide can participate in the O_2 formation on some surfaces (e.g. gold or ruthenium oxide) [25, 26], while on others O_2 forms only from water adsorbed at the surface (e.g. platinum oxide) [27].

All noble metal oxides are unstable towards dissolution under the highly oxidizing potentials of the OER. The combination of electrochemistry with online elemental analysis of the electrolyte has shown that the dissolution of precious metals and their oxides must be distinguished between steady and transient dissolution, i.e. during potentiostatic or potentiodynamic conditions respectively [21]. Transient dissolution occurs mostly during the reduction of the metal oxide, and to a lesser extent during the reverse oxidative transition, but always during changes in the metal or metal oxide state. On the contrary, steady dissolution occurs with a constant rate at a fixed potential or current. IrO_2 and RuO_2 exhibit transient dissolution, while the steady dissolution (relevant for the OER) is very pronounced for RuO_2 only (see Fig. 3), due to the oxidation of the rutile-type RuO_2 phase to RuO_4 [28, 29]. The same trend is maintained also in alkaline solution, where the absolute dissolution rates are actually higher compared to acidic for either IrO_2 or RuO_2 [30, 31]. Therefore, despite its slightly higher overpotential for the OER, IrO_2 is the state-of-the-art catalyst for the OER because of its better stability compared to

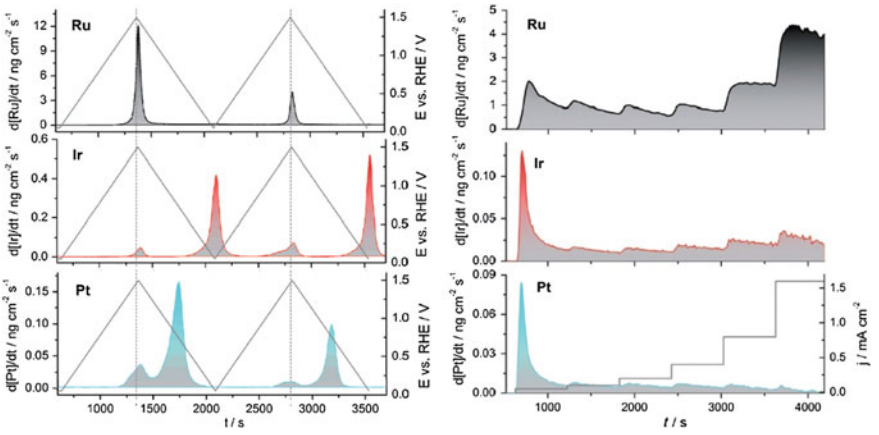

Fig. 3 Online monitoring of the dissolution rate of polycrystalline Ru, Ir and Pt during (*left*): potential ramps from 0.05 to 1.5 V_{RHE} with 2 mV s^{-1} and (*right*): galvanostatic polarization from 0.05 to 1.6 mA cm^{-2}. Electrolyte: 0.1 M H_2SO_4. Reproduced from [21] with permission from Wiley

RuO_2. One other approach to combine the higher activity of RuO_2 and the better stability of IrO_2 has been to use mixed ruthenium–iridium oxides [32, 33].

By decreasing the particle size of nanoparticulate RuO_2 or IrO_2 catalysts, not only the surface-to-volume ratio but also the area-normalized OER activity increases [34–36]. This trend has been attributed to the higher proportion of less active ordered planes at larger particles [34–36]. Therefore, in terms of mass-normalized activity the goal for RuO_2 or IrO_2 catalysts is to decrease the particle size. The stability, however, of the state-of-the-art IrO_2 catalysts decreases with decreasing the particle size [36].

Because of the amount of precious iridium needed for IrO_2 catalysts, approaches to reduce the iridium content by mixing it with another non-noble material have been explored. For instance, Nd_3IrO_7 or $Pb_2(Pb_xIr_{2-x})O_{7-y}$ were found to be about as active as IrO_2 in strongly alkaline solutions [37]. Double perovskites based on iridium and a second metal oxide, such as Ba_2NdIrO_6, can combine up to three times improved OER activity in acid and three times lower noble metal content compared to state-of-the-art IrO_2, while the stability of these materials is comparable to IrO_2 [38].

However, the main approach to replace expensive and scarce noble metals has been to develop catalysts based entirely on non-noble transition metals. In acidic solutions, IrO_2 clearly outperforms these materials which are additionally not stable (see Fig. 4). Therefore, the electrolyte for non-noble OER catalysts typically needs to be neutral or alkaline, since the dissolution of the electrode is minimal and the OER activity similar to that of IrO_2 in this medium (see Fig. 4). Neutral electrolytes, however, are expected to face issues of lower conductivity and local pH changes even for strongly buffered solutions. Different classes of such materials

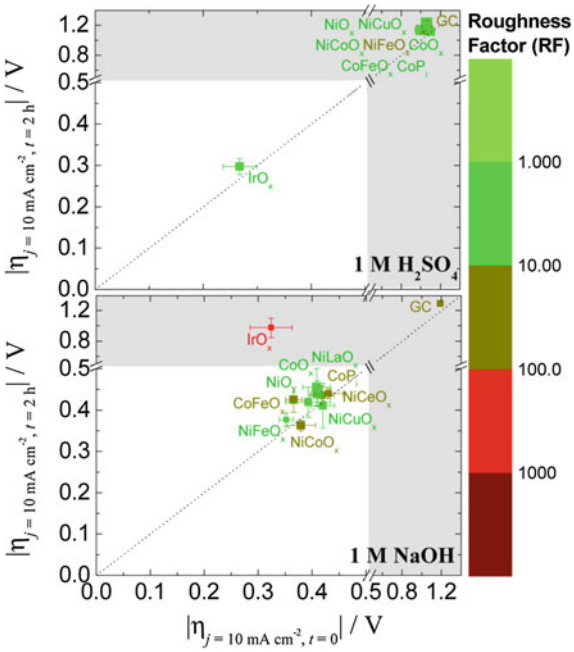

Fig. 4 Plots of catalytic activity, stability, and electrochemically active surface area for OER electrocatalysts in acidic (*top*) and alkaline (*bottom*) solutions. The x-axis and y-axis show the overpotential required to achieve 10 mA cm^{-2} per geometric area at time t = 0 and t = 2 h. The *diagonal dashed line* is the expected response for a stable catalyst. The *unshaded white region* highlights the region where the overpotential to achieve 10 mA cm^{-2} at time t = 0 and 2 h is < 0.5 V. Note the break and change in scale in both axes at overpotentials > 0.5 V. Reprinted from Ref. [40] with permission from the American Chemical Society

have been investigated; for example, rutile-type Co-, Ni- and Mn-based oxides, the activity of which increases in 0.1 M KOH in the order $MnO_x < NiO_x < CoO_x$ and they are somewhat less active compared to IrO_x [39, 40]. This activity trend is explained in terms of the oxygen binding energy of the materials [24]. Interestingly, the activity of mixed oxides such as $NiCoO_x$, $NiFeO_x$, $CoFeO_x$, etc. is higher than the activity of the individual metal oxides, almost approaching that of IrO_2 in the same solution [40]. Other interesting classes of materials are spinel- or perovskite-type electrodes. The first systematic investigations on spinels such as $NiCo_2O_4$, $NiLa_2O_4$, Co_3O_4, etc. were made by Tseung and by Trasatti in alkaline solutions [41–43]. Early studies on ABO_3 perovskites (A: a lanthanide, B: a first-row transition metal) were carried out by Bockris, who tried to identify the parameters that control the electrocatalytic activity. Bockris proposed that the rate-determining step is the desorption of OH and hypothesized that the OER activity of perovskites follows a volcano-type relationship where the activity descriptor is the adsorption energy of OH on the transition metal used in the perovskite [44, 45]. The analysis of Bockris already allowed the early prediction of

some active perovskites, such as $LaNiO_3$ or $LaCoO_3$ [45]. Using molecular orbital principles, Shao-Horn and co-workers [46] first derived a volcano-type relationship for a series of perovskite-type oxides of first-row transition metals and then predicted that $Ba_{0.5}Sr_{0.5}Co_{0.8}Fe_{0.2}O_{3-\delta}$ (BSCF) will be located at the top of this volcano. The very high activity of this material was verified experimentally, and it is by 10 times higher than the state-of-the-art IrO_2 in alkaline solution. The same group later showed that the BSCF particles in fact undergo quick amorphization during the oxygen evolution, which leads to an activity increase [47].

Another approach, finally, is the so-called "in situ formed" catalysts. Starting from a neutral, phosphate-buffered Co^{2+}-containing solution and an indium tin oxide (ITO) substrate, Kanan and Nocera showed that oxygen is evolved at positive bias, probably through the oxidation of Co^{2+} to Co^{3+}, precipitation of Co^{3+}–HPO_4^{2-} on the ITO, and consequent oxidation of Co^{3+} to Co^{4+}. The in situ grown film on the ITO is active for the OER and the formed Co^{4+} is reduced to Co^{2+}, so a new catalysis round can start [48].

4 Oxygen Reduction Reaction

Of all the monometallic catalysts, platinum exhibits the highest activity for the ORR, being located closest to the top of the volcano [49]. The trends in the ORR activity for model low- and high-index single-crystal surfaces depend on the electrolyte, which highlights the importance of the structure-sensitive adsorption of electrolyte ions on platinum. In particular, the ORR activity increases in the order (100) < (111) ≈ (110) in $HClO_4$, (111) < (100) < (110) in H_2SO_4 and (100) < (110) < (111) in KOH [50–53]. The activity of (111) increases by the introduction of (111) or (100) steps in $HClO_4$ and H_2SO_4, but has the opposite effect in KOH [13, 54]. On the other hand, the activity of (100) is not influenced by the introduction of (111) or (110) steps in $HClO_4$ and H_2SO_4, but increases in KOH [13, 54]. The sensitivity of the ORR activity on the surface atom arrangement indicates that the platinum activity can be tuned by finding the appropriate surface geometry. Indeed, high-index facets are more active than the low-index crystals in $HClO_4$, with Pt(331) and Pt(221) being the most active of all [51].

To enhance the utilization of platinum atoms in a real system, the ratio of surface to bulk atoms (surface-to-volume ratio) needs to increase using for instance finely dispersed platinum nanoparticles on a high-surface-area support. However, the decrease of the particle size does not merely increase the surface-to-volume ratio: the properties of surface atoms at nanoscale are different than in extended surfaces due to structural and electronic effects. The origin of such effects lies in the size- and shape-dependent distribution of surface atoms to various short- and long-range terraces and to different steps and defect sites [55–57]. To develop design rules for ORR catalysts from pure platinum, the impact of surface atom arrangement must be rationalized, e.g. by the introduction of activity descriptors that include structure-sensitive parameters such as the generalized coordination numbers [58, 59].

If the particles are represented as truncated octahedra, then the ratio of surface atoms on (111) and (100) terraces decreases for smaller particles [60, 61]. This is predicted to decrease the area-normalized activity toward the ORR, especially in the size range 2–10 nm (particle size effect) [60, 61]. Such a prediction has been confirmed experimentally only when uniformly defined ultrathin catalyst layers are prepared; such layers prevent any O_2 diffusion limitations within the catalyst layer [62, 63]. The mass-normalized activity is a trade-off between the better Pt utilization and the lower reaction rate by decreasing the particle size. Thus, the mass-normalized activity is maximized at ca. 3 nm [63, 64], which is the typical size for state-of-the-art carbon-supported Pt catalysts for the ORR.

The orientation of surface atoms can be also altered by the nanostructure shape. For instance, nanoparticles with dominant (100) terraces (e.g. cubic particles) are more active in H_2SO_4 but those with dominant (111) terraces (e.g. cubooctahedral or tetrahedral particles) are more active in $HClO_4$ and KOH. This is consistent with the fact that Pt(100) is more active than Pt(111) only in H_2SO_4 [65, 66]. Nanoparticles that exhibit a high proportion of high-index facets are in general much more active than particles of a similar size [67–69], which is attributed to the higher activity of high- versus low-index facets. The stability of shape-controlled nanoparticles under the ORR conditions is however an issue, especially for those enclosed by high-index facets, and eventually these particles reshape due to degradation issues that will be discussed below [70, 71].

Even though the ORR takes place at potentials below +1.0 V_{RHE}, the biggest challenge currently for Pt-based ORR catalysts is their exposure to potentials at which the catalyst or the catalyst support is unstable [72]. The cathode transiently experiences potentials as high as 1.4 V during start-up or shut-down of the fuel cell, as a result of the reverse-current decay mechanism [73]. Since the long-term performance is affected by processes during the entire operation, from start-up to regular load to shut-down, assessing the stability of ORR catalysts for a potential up to 1.5 V represents better the conditions in a fuel cell. Platinum dissolves mostly transiently, i.e. during the reduction of the metal oxide. Apart from metal dissolution, real ORR catalysts can suffer from other degradation mechanisms which are induced by the catalyst exposure to highly positive potentials [74, 75]: (i) particle migration and coalescence, (ii) dissolution of platinum from small particles and redeposition at larger particles (Ostwald ripening) and (iii) corrosion of the support which enhances particle mobility and detachment. The above mechanisms, which may take place in parallel [75], eventually result in a loss of platinum surface area. In addition, the dissolved platinum from the cathode may be reduced by hydrogen that permeates through the membrane, forming a large "Pt band" on the membrane [76].

A particularly interesting class of platinum materials that are aimed to mitigate stability issues are the "nanostructured thin-film" (NSTF) electrocatalysts innovated by 3M. They consist of non-conductive organic crystalline whiskers as the support, on which an ultrathin layer of platinum is deposited [77]. The polycrystalline thin-film catalyst morphology and the absence of a conventional conductive high-surface-area carbon support allow the NSTF catalysts to combine a

polycrystalline-like surface-normalized ORR activity, with a low amount of noble material required and an improved stability, since they are free from issues such as support corrosion, Pt particle migration and coalescence, etc. [77, 78]. However, the catalyst morphology introduces also disadvantages, such as the higher susceptibility to flooding at low temperature of operation, which decreases limiting currents and makes water management more complicated.

Returning to the volcano plot, the problem with platinum is that it binds oxygen a bit too strongly, i.e. it is located at the left side of the ORR volcano in Fig. 2 [79, 80]. In a series of patents from the United Technologies Corporation (UTC) in 1980s, it was disclosed that binary or ternary PtCr, PtV or PtCrCo alloys are more active for the ORR than pure platinum [81–85]. Since then, the strategy to weaken the Pt–O bond to move closer to the top of the volcano has been to use such Pt–M catalysts, where M is a late transition metal such as Cu, Ni, Co, Fe, etc. (see Fig. 2) [79, 86–91] or alloys with more than one alloying element [92–94]. Alloying platinum leads to a modification of the surface electronic properties, even though the atoms of the alloying metal are not present at the surface as they are not stable under the ORR conditions when in contact with the electrolyte. The enhancing effect of the alloying metal atoms to the intrinsic ORR activity has been attributed to bonding interactions between surface Pt and sub-surface M atoms (electronic or ligand effect), and to the compressed arrangement of the surface Pt atoms due to the shorter M–M interatomic distance below the surface (geometric or strain effect) [89, 91]. Even though it is hard to decouple the two effects, the consequence of both is to alter the chemisorption properties of the surface Pt atoms, and the alloying metal atoms have a stronger impact when they are located closer to the surface (see Fig. 5) [90, 91, 95, 96]. Therefore, ideally the alloying M metal must be located in the second layer.

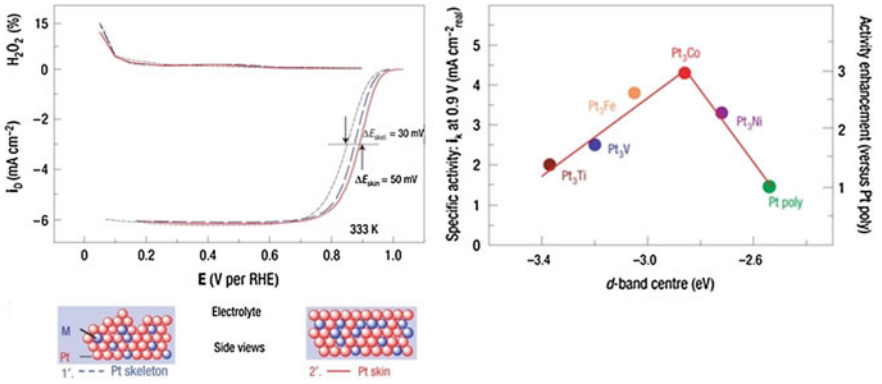

Fig. 5 *Left* Polarization curves for the ORR on polycrystalline platinum (*grey curve*), skeleton-Pt_3Fe (*blue dashed curve*) and skin-Pt_3Fe (*red curve*), in 0.1 M $HClO_4$ at 50 mV s^{-1}. *Right* Volcano-type plots of the experimentally measured ORR activity for various skin-Pt_3M surfaces at a temperature of 333 K. Reproduced from Ref. [91] with permission from the Nature Publishing Group

The activity enhancement for bimetallic Pt surfaces may depend strongly on the surface atom arrangement: for Pt_3Ni-skin[2] surfaces in $HClO_4$, the ORR activity increases by ca. 9 times for the $Pt_3Ni(111)$ versus Pt(111) and by only 2–2.5 times for $Pt_3Ni(100)$ versus Pt(100) or for $Pt_3Ni(110)$ versus Pt(110) [97]. This alters the order in which the ORR activity increases, from Pt_3Ni-skin(100) to Pt_3Ni-skin(110) to Pt_3Ni-skin(111) in $HClO_4$ (compare with Pt(100) < Pt(111) ≈ Pt(100) in the same solution) [97].

The situation is rather complex for nanoparticulate bimetallic catalysts, when the goal is to obtain the maximum possible activity enhancement. The preparation method and the post-treatment can have a significant impact on parameters such as the size or the shape of the nanostructure, porosity, alloy composition, etc., which in turn influence the ORR performance. As expected from the findings on extended bimetallic surfaces described above, the ORR activity enhancement depends strongly on the shape of the nanostructure. The ORR activity on carbon-supported octahedral Pt_3Ni particles (i.e. with a high ratio of (111) terraces) is by ca. 7 times higher than the commercial Pt/C catalyst, whereas cubic Pt_3Ni particles (i.e. with a high ratio of (100) terraces) show little enhancement [98].

To increase platinum utilization, to decrease the amount of noble metal needed, and to maximize the alloying effect, the approach that gained the largest interest is the synthesis of nanostructures with a pure Pt shell and a Pt–M core, so-called core–shell materials. The Pt shell is supposed additionally to protect the non-noble M metal atoms in the core, where M is typically a late transition metal such as Cu, Co, Ni, etc. However, as it will be described below, this is not really the case. Nanostructures with a highly ordered core are more active and stable than disordered particles [99–103] with the explanation being still under debate. For a detailed description of the methods for the preparation of core–shell structures the interested reader is referred to relevant reviews [104, 105]. In the following, we will briefly mention only the two main preparation methods:

In dealloying, the less noble metal atoms of a bimetallic alloy are rapidly and selectively dissolved. Classical dealloying involves the selective dissolution of the less noble metal, i.e. of the metal with the least positive standard reduction potential [106, 107]. The Strasser group showed that core–shell nanoparticles can be prepared by an "electrochemical dealloying" process, in which an M-rich platinum alloy precursor, e.g. $PtCu_3$, is subject to cycling within a potential region where M is unstable [89, 108, 109]. The interesting feature of dealloyed core–shell particles is that the resulting structure and its activity/stability can be controlled by parameters such as the initial alloy composition, the dealloying or post-treatment conditions, the size of the particle precursor, etc. [109].

[2] *Pt-skeleton* is the surface that remains after the dissolution of M metal atoms from Pt–M alloys exposed to oxidizing conditions. *Pt-skin* is the surface which consists of a pure topmost atomic Pt layer.

Another method of core–shell preparation is based on the spontaneous galvanic replacement of the non-noble material at the surface of the core by platinum. This can be achieved using PdM (e.g. PdCu, PdCo) cores which result in a PdCu@Pt or PdCo@Pt core–shell structure. Adzic and co-workers pioneered a more elegant method of galvanic replacement, the so-called monolayer method; a copper monolayer, formed by underpotential deposition on the surface of an M metal core, is spontaneously oxidized by platinum ions which are reductively deposited. This results in a core–shell structure with a monolayer of platinum enclosing an M core. The metal core M can be Pd, Au, Ir, or even bimetallic such as PdNi. The method was originally developed on model single-crystalline "cores" and extended to nanostructured electrodes [90, 110–112].

Except for core–shell structures, other interesting approaches for the preparation of bimetallic materials include alloys based on 3M's NSTF technology (e.g. Pt_3Ni_7-NSTF) [113] or the Pt_3Ni-skin nanoframes [114]; the latter enhance the ORR activity by 16 times compared to standard Pt/C catalysts.

The stability of bimetallic electrodes is an important issue, which limits their application in real systems. The dissolution of platinum removes Pt surface atoms from the protective shell, leading to the exposure of the otherwise protected non-noble metal atoms to the electrolyte [115]. This eventually results in the dissolution of the alloying metal atoms from the first atomic layers and the thickening of the protective Pt shell, so the enhancing effect from alloying decays with time. Even worse is the fact that the dissolved metal ions deteriorate the fuel cell performance further. For example, copper ions can be reduced and deposited at the anode of the fuel cell [116], while nickel or cobalt ions can be deposited on the membrane [113, 117].

DFT calculations predicted that alloys of platinum with rare earths (e.g. Pt_3Y and Pt_3Sc) will be not only more active, but also more stable than pure platinum or other Pt alloys [80]. The argumentation is based on the higher (more negative) enthalpy for alloy formation of such alloys compared to those with late transition metals, which is likely to render the diffusion of the alloying metal to the surface kinetically more difficult [80, 118]. The correlation between the enthalpy for alloy formation and the kinetic barrier for diffusion of the alloying element has been demonstrated in a later publication [119]. The higher activity of model Pt_5M alloys (M: a rare earth or alkaline earth element such as Sc, Y, La, etc.) for the ORR was evidenced experimentally by the Chorkendorff group and was attributed to strain [118, 120–122]. The same group also showed the enhanced activity with nanostructured electrodes [123, 124]. Long-term accelerated degradation tests on such catalysts indeed showed that the selective dissolution of the second metal is slower; however, there is still an activity loss with time and a concomitant thickening of the platinum shell, for either extended or nanostructured surfaces [120, 125].

Due to the high cost and the limited crustal abundance of platinum, extensive efforts to find alternative catalysts have been made. A good alternative to platinum would exhibit high activity for the ORR, low cost, sufficient abundance and stability under the operation conditions of a fuel cell.

Among other monometallic surfaces, mostly palladium has been considered as a potential candidate. Palladium is the metal closest to platinum in the volcano plot and its price is lower. For flame-annealed palladium single-crystal electrodes, the ORR activity increases in the order Pd(110) < Pd(111) < < Pd(100) [126]. The trend may be different for Pd(hkl) crystals annealed by other methods, e.g. inductive heating [127]. Overall, the problems with palladium are that (i) its activity must still increase to compete with platinum, (ii) it is significantly more susceptible to dissolution than Pt [21] and (iii) it is still a rather scarce metal, so a large-scale technology would increase the demand and the price for Pd substantially.

Other approaches include the use of noble metal-free catalysts, such as chalcogenides, oxides, carbides, nitrides, etc. [128]. The activity of such materials, however, remains low compared to platinum. The most promising way to replace platinum with catalysts free of noble metals is a class of materials noted generally as $Me–N_x/C_y$, where Me is a transition metal, for example, iron (Fig. 6) [129]. The first report on such materials showed that cobalt phthalocyanine can reduce O_2 in acidic solution; [130] later it was shown that also other $Me–N_4$ chelates can catalyse the reaction in either acid or alkaline [131, 132]. The activity of those catalysts was decreasing with time because of catalyst decomposition by the formed H_2O_2 but thermal treatment improves the stability of the catalyst likely by making it more active for H_2O_2 decomposition [133, 134]. It has been, however, questionable whether the metal centre is still a component of the active site or if the pyrolysis results in a new catalyst, consisting of nitrogen and carbon [135–138]. Yeager and co-workers showed later that it is not necessary to use $Me–N_4$ chelates as the precursor, but the catalyst can also be synthesized at high temperature by mixing a Me salt with a carbon–nitrogen source [139], while Dodelet and co-workers showed that the sources of carbon and nitrogen can be also different [140].

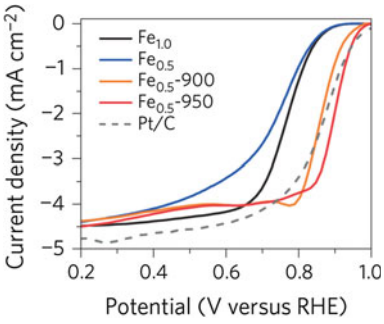

Fig. 6 ORR polarization curves for Fe–N–C catalysts and a Pt/C benchmark catalyst, recorded at room temperature in O_2-saturated pH 1 electrolyte at a rotation rate of 1,600 rpm. The current was corrected for the background current measured in N_2-saturated electrolyte. The potential was corrected for the Ohmic drop. The catalyst loadings were 818 $\mu g_{Fe\text{-}N\text{-}C}$ cm^{-2} or 16 μg_{Pt} cm^{-2}. The *subscript* shows the wt% Fe in the catalyst precursor, i.e. prior to any pyrolysis; $Fe_{0.5}$-900 and $Fe_{0.5}$-950 were obtained after pyrolysis of $Fe_{0.5}$ at 900 °C or 950 °C, respectively. Reproduced from Ref. [129] with permission from the Nature Publishing Group

The above progress indicated that (i) an important parameter for this class of materials is the density of Me–N_4 sites per unit volume, independent of whether they serve as the active sites or as the precursors for the generation of active sites after pyrolysis and (ii) the design of catalyst can be tailored by the careful choice of the transition metal, the nitrogen, and the carbon source as these can be independently added, as well as by following appropriate treatment procedures.

Following this notion, the Dodelet group synthesized a very active Fe–N/C catalyst by increasing substantially the density of active sites [141]. They used initially a mixture of a highly (micro)porous carbon support, a pore filler and ferrous acetate, which was subject to ball milling to force the pore filler and the iron precursor into the pores, and then was pyrolyzed first in Ar and then in NH_3 to generate the Fe–N_4 moieties on the carbon support. The high density of such moieties makes this catalyst active for the ORR, so the activity reaches the ca. 90% of the activity of Pt/C [141]. The Zelenay group used heteroatom polymer precursors such as polypyrrole (PPy) or polyaniline (PANI) as the template for nitrogen and carbon, aiming to a uniform distribution and high density of Me–N_4 sites. They initially showed that Co–PPy/C catalyst exhibits respectable stability and activity without any pyrolysis step [142]. Later, they synthesized pyrolyzed Fe-, Co- and FeCo-PANI/C catalysts with activity that almost matches the one of Pt/C and promising stability which was proposed to be due to a graphitized carbon phase [143].

The ORR activity and selectivity on Me–N_4 chelates (where Me: Fe, Mn, Co) is related to the binding energy of O_2, which in turn follows the redox potential for the Me(III)/Me(II) transition [144]. Catalysts with weak O_2 binding (i.e. positive redox potential) reduce O_2 to H_2O_2 and the onset potential shifts more positive in the RHE scale by making the solution more alkaline. On the other hand, catalysts with strong O_2 binding (i.e. negative redox potential) reduce O_2 to H_2O_2 and the onset potential is independent of the pH in the RHE scale.

Overall, the progress made in the last ten years in ORR catalysis with non-noble metals is impressive [128, 145]; however, the issue of stability and long-term performance remains. In fact, non-noble metal catalysts also suffer from degradation when they are exposed to potentials above 0.9 V in acidic solutions. The main origin of degradation is the oxidation of carbon, which leads to the destruction the ORR-active FeN_xC_y sites, while iron leaching from iron particles occurs already at lower potentials (<0.7 V) without though affecting the ORR activity [146].

5 Fundamentals of the HER and the HOR

The hydrogen evolution and the reverse oxidation reaction involve the transfer of two electrons:

$$2H^+ + 2e^- \rightleftarrows H_2 \quad E = 0\,V\,vs\,RHE. \tag{16}$$

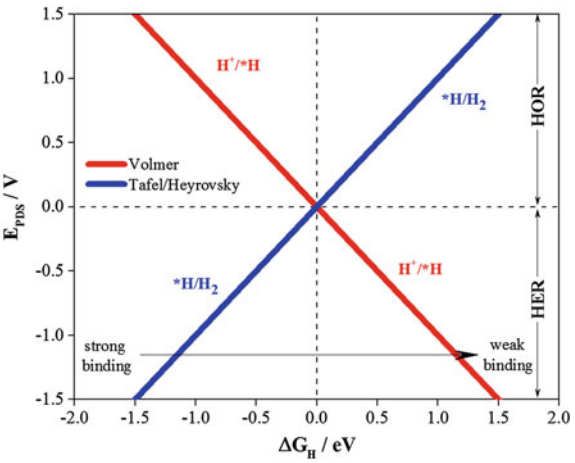

Fig. 7 Thermodynamic volcano plots for the HER and the HOR, with the energy of hydrogen adsorption as the descriptor, assuming a Volmer-Tafel/Heyrovsky pathway. Reproduced from [15] with permission from Elsevier

The generally accepted mechanism for the HER/HOR involves the following three elementary steps [147]:

$$H^+ + * + e^- \rightleftarrows H_{ads} \quad \text{Volmer step} \tag{17}$$

$$H_{ads} + H^+ + e^- \rightleftarrows H_2 \quad \text{Heyrovsky step} \tag{18}$$

or

$$2H_{ads} \rightleftarrows H_2 + 2^* \quad \text{Tafel step.} \tag{19}$$

Thus, both reactions involve the intermediate formation of H_{ads}, the binding energy of which can be used as a descriptor for the construction of volcano plots (Fig. 7), following a similar analysis as for the OER/ORR. The ideal catalyst for both reactions adsorbs hydrogen with $\Delta G_{*H} = 0$, meaning that the energy of *H is the same as that of H_2 and H^+. In that case, there are no uphill or downhill steps during any of the two electron transfer steps in the corresponding energy diagram, and thus this ideal case is associated with zero overpotential. If the binding is too strong ($\Delta G_H < 0$), then the two reactions are associated with overpotential, because the Heyrovsky/Tafel step limits the HER and the Volmer step limits the HOR. The opposite occurs for too weak *H binding ($\Delta G_H > 0$).

6 Hydrogen Evolution Reaction

Trasatti has provided the most traditional expression of a kinetic volcano for the HER [148], using the M–H bond energy as the activity descriptor. Platinum and other Pt-group metals are located near or at the top of the volcano. In the interpretation of

such an expression, however, one should take into account that the energies of *H adsorption were calculated for bare metal surfaces, which is not really representative of the conditions during the HER on all metals [149].

In fact, platinum catalyses the HER in acidic solutions with a very high rate, so that the current is entirely limited by H^+ diffusion [150, 151]. Therefore, conventional RDE measurements cannot be used to estimate the kinetics of the HER on platinum [151]. Moreover, no significant impact of the surface structure was found for the HER on low-index Pt single crystals in acid [152]. The development of platinum-free HER catalysts in acid has been explored to replace platinum in acid electrolyzers, with sulfides, carbides or phosphides being the most promising materials [153].

Contrary to acidic solutions, platinum is not as good a catalyst in alkaline (see Fig. 8) [151]. The reaction is structure sensitive on Pt, which also contrasts with acidic solutions, with the activity increasing in the order Pt(111) < Pt(100) < Pt (110) [154]. The reason for the observed structure sensitivity only in alkaline solutions and for the lower reaction rate compared to acid is still unknown [155]. The lower activity of Pt in alkaline solution implies higher cell voltage in an alkaline electrolyzer, thus other catalysts must be developed to carry out the reaction in alkaline solutions as fast as platinum does in acid. Nickel is a state-of-the-art catalyst for the HER in alkaline solution [156]; however, the catalyst deactivates and the cell voltage increases in the long term [157], which has been attributed to the formation of hydrides [158]. One approach has been to modify platinum with $Ni(OH)_2$ clusters, which was found to increase the HER activity in alkaline compared to pure Pt by a factor of 8 [155]. The promoting effect of this modification was attributed to the enhancement of water splitting by $Ni(OH)_2$, while *H recombination still occurs on platinum, in a reaction that proceeds in a bifunctional manner.

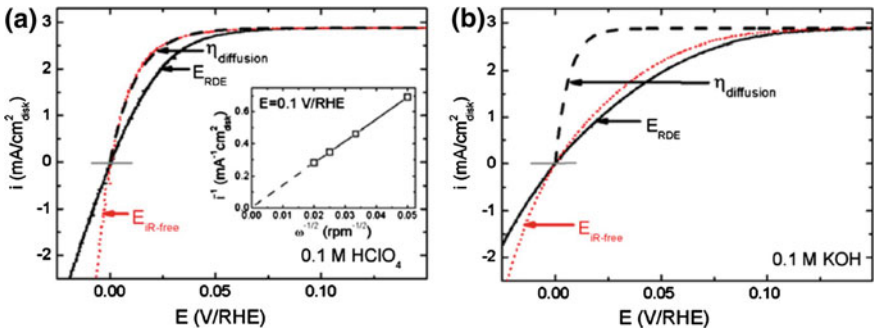

Fig. 8 HOR/HER polarization curves on polycrystalline platinum in 0.1 M $HClO_4$ (**a**) and 0.1 M KOH (**b**) at 1600 rpm. *Solid black curves* represent the voltammograms before iR-correction (E_{RDE}), *dotted-red lines* after iR-correction (iR-free) and *dashed black curves* the Nernstian diffusion overpotential. Reprinted from Ref. [151] with permission from the Electrochemical Society

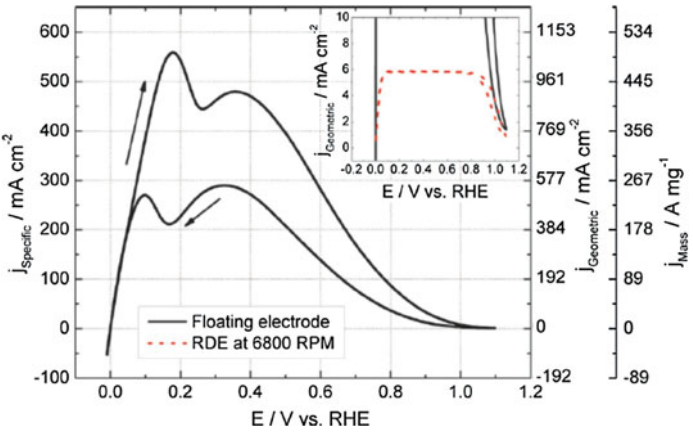

Fig. 9 HOR polarization curves using a "floating electrode" with a 2.2 μg cm^{-2} Pt/C catalyst exposed to H_2, run in 4.0 M $HClO_4$, at 10 mV s^{-1}. The *inset* shows the comparison of the floating electrode measurement with the HOR on polycrystalline platinum using an RDE (6800 rpm) in 0.5 M $HClO_4$. Reprinted from Ref. [160] with permission from the Royal Society of Chemistry

7 Hydrogen Oxidation Reaction

Platinum catalyses also the HOR with a very high rate in acid, so that the current is entirely limited by H_2 diffusion [150, 151]. The reaction is so fast that the current is fully preserved even when the surface of platinum is covered by a surface modifier such as calix[4]arene to a coverage of 98% [159]. Similar to the HER, the high reaction rate makes it impossible to correctly measure kinetics for the HOR with RDE measurements. Following the concept of the "floating electrode"[3] which allows extremely high mass transport rates of a gaseous reactant, Kucernak and co-workers managed to record HOR curves with limited hydrogen mass transport limitations [160], and the measured current densities were in the order of 0.5 A cm_{Pt}^{-2} (Fig. 9).

Similar to the HER, the HOR deviates from the ideal Nernstian behaviour in alkaline solutions on platinum [151]. Indeed, the reaction is structure sensitive only in alkaline media, with the activity increasing in the order Pt(111) ≈ Pt(100) << Pt (110) at low positive overpotential [154]. At high potentials, the inhibition from the adsorption of oxygenated species is stronger for Pt(100) and weaker for Pt(111) [154]. The lower rate of the HOR in alkaline solution implies that a higher amount of Pt (about 100 times) is required in an alkaline fuel cell to achieve the same

[3]The "floating electrode" is a three-electrode setup that consists of a porous gas diffusion working electrode floating on an aqueous electrolyte. The reference and counter electrodes are immersed into the solution. The reactant gas is supplied to the catalyst surface sites from the gas phase, on top of the floating catalyst layer. The gaseous diffusion leads to extremely fast mass transport of reactant gases to the catalyst layer.

performance as for an acidic fuel cell. Nickel-based catalysts are the only materials to date, to be successful in achieving HOR activities comparable to platinum in alkaline solutions [161].

8 Summary

In conclusion, the electrocatalysis community has developed a good understanding of the reactions involved in the hydrogen economy; the HER and OER for water electrolyzers, and the HOR and ORR for fuel cells. The activity of each reaction on different surfaces follows a volcano-type relationship where the adsorption energy of a key reaction intermediate can be used as the descriptor, for example, *H for HOR and HER and *O for ORR and OER. The highest activity is obtained for a catalyst that exhibits moderate *H or *O binding, accordingly. However, for reactions involving more than one intermediate (and typically involving more than two electron and proton transfers), such as ORR and OER, energetic scaling relations between intermediates (specifically *O, *OH and *OOH) limit the extent to which a reversible catalyst with a very small overpotential can be achieved. A minimal overpotential of ca. 0.25–0.3 V for both ORR and OER appears very difficult to overcome. Computational and experimental tools offer today the opportunity to prepare highly active materials that approach the performance of the optimal catalyst predicted by current models. However, future models and computational methods should focus on materials that can break the energetic scaling relations between intermediates, to develop catalysts with significantly enhanced properties compared to the current state-of-the-art electrocatalysts.

Despite the massive efforts that have been devoted to the development of materials that operate in alkaline environments and with lower/no noble metal content, the best systems remain to be acidic water electrolyzers or fuel cells, using Pt for the HER, the HOR and the ORR, and IrO_2 for the OER. However, such systems can be a solution only for the small scale: to realize Bockris' hydrogen economy on a large scale we need to find a combination of materials for the two electrodes that are abundant and but also stable in the long term. This is today the biggest challenge, as it will decrease the cost per device, but will also massively increase the number of devices that can be used worldwide.

References

1. Verne J (1874) The mysterious island
2. Bockris JO (1972) A hydrogen economy. Science 176:1323–1323
3. van Troostwijk AP, Deiman JR (1789) Sur une manière de décomposer l'eau en air inflammable & en air vital. Obs Phys 35:369–378
4. Grove WR (1839) On voltaic series and the combination of gases by platinum. Philos Mag 14:127–130

5. Schönbein CF (1839) On the voltaic polarization of certain solid and fluid substances. Philos Mag 14:43–45
6. Kinoshita K (1992) Oxygen electrochemistry. Electrochemical oxygen technology. Wiley, New York, pp 19–112
7. Nilekar AU, Mavrikakis M (2008) Improved oxygen reduction reactivity of platinum monolayers on transition metal surfaces. Surf Sci 602:L89–L94
8. Dau H, Limberg C, Reier T et al (2010) The mechanism of water oxidation: from electrolysis via homogeneous to biological catalysis. ChemCatChem 2:724–761
9. Katsounaros I, Cherevko S, Zeradjanin AR, Mayrhofer KJJ (2014) Oxygen electrochemistry as a cornerstone for sustainable energy conversion. Angew Chem Int Ed 53:102–121
10. Katsounaros I, Schneider WB, Meier JC et al (2012) Hydrogen peroxide electrochemistry on platinum: towards understanding the oxygen reduction reaction mechanism. Phys Chem Chem Phys 14:7384–7391
11. Katsounaros I, Schneider WB, Meier JC et al (2013) The impact of spectator species on the interaction of H_2O_2 with platinum—implications for the oxygen reduction reaction pathways. Phys Chem Chem Phys 15:8058–8068
12. Sitta E, Gómez-Marín AM, Aldaz A, Feliu JM (2013) Electrocatalysis of H_2O_2 reduction/oxidation at model platinum surfaces. Electrochem Commun 33:39–42
13. Gómez-Marín AM, Rizo R, Feliu JM (2013) Some reflections on the understanding of the oxygen reduction reaction at Pt(111). Beilstein J Nanotechnol 4:956–967
14. Rossmeisl J, Logadottir A, Nørskov JK (2005) Electrolysis of water on (oxidized) metal surfaces. Chem Phys 319:178–184
15. Koper MTM (2011) Thermodynamic theory of multi-electron transfer reactions: implications for electrocatalysis. J Electroanal Chem 660:254–260
16. Rossmeisl J, Karlberg GS, Jaramillo T, Nørskov JK (2009) Steady state oxygen reduction and cyclic voltammetry. Faraday Discuss 140:337–346
17. Rossmeisl J, Qu Z-W, Zhu H et al (2007) Electrolysis of water on oxide surfaces. J Electroanal Chem 607:83–89
18. Koper MTM (2013) Analysis of electrocatalytic reaction schemes: distinction between rate-determining and potential-determining steps. J Solid State Electrochem 17:339–344
19. Bligaard T, Nørskov JK, Dahl S et al (2004) The Brønsted–Evans–Polanyi relation and the volcano curve in heterogeneous catalysis. J Catal 224:206–217
20. Trasatti S (1980) Electrocatalysis by oxides—attempt at a unifying approach. J Electroanal Chem 111:125–131
21. Cherevko S, Zeradjanin AR, Topalov AA et al (2014) Dissolution of noble metals during oxygen evolution in acidic media. ChemCatChem 6:2219–2223
22. Reier T, Oezaslan M, Strasser P (2012) Electrocatalytic oxygen evolution reaction (OER) on Ru, Ir, and Pt catalysts: a comparative study of nanoparticles and bulk materials. ACS Catal 2:1765–1772
23. Lee Y, Suntivich J, May KJ et al (2012) Synthesis and activities of rutile IrO_2 and RuO_2 nanoparticles for oxygen evolution in acid and alkaline solutions. J Phys Chem Lett 3:399–404
24. Man IC, Su H-Y, Calle-Vallejo F et al (2011) Universality in oxygen evolution electrocatalysis on oxide surfaces. ChemCatChem 3:1159–1165
25. Wohlfahrt-Mehrens M, Heitbaum J (1987) Oxygen evolution on Ru and RuO_2 electrodes studied using isotope labelling and on-line mass spectrometry. J Electroanal Chem 237:251–260
26. Diaz-Morales O, Calle-Vallejo F, de Munck C, Koper MTM (2013) Electrochemical water splitting by gold: evidence for an oxide decomposition mechanism. Chem Sci 4:2334–2343
27. Willsau J, Wolter O, Heitbaum J (1985) Does the oxide layer take part in the oxygen evolution reaction on platinum? J Electroanal Chem 195:299–306
28. Yeo RS, Orehotsky J, Visscher W, Srinivasan S (1981) Ruthenium-based mixed oxides as electrocatalysts for oxygen evolution in acid electrolytes. J Electrochem Soc 128:1900–1904

29. Kötz R, Stucki S, Scherson D, Kolb DM (1984) In-situ identification of RuO_4 as the corrosion product during oxygen evolution on ruthenium in acid media. J Electroanal Chem 172:211–219
30. Cherevko S, Zeradjanin AR, Keeley GP, Mayrhofer KJJ (2014) A comparative study on gold and platinum dissolution in acidic and alkaline media. J Electrochem Soc 161: H822–H830
31. Cherevko S, Geiger S, Kasian O et al (2016) Oxygen and hydrogen evolution reactions on Ru, RuO_2, Ir, and IrO_2 thin film electrodes in acidic and alkaline electrolytes: a comparative study on activity and stability. Catal Today 262:170–180
32. Kötz R, Stucki S (1986) Stabilization of RuO_2 by IrO_2 for anodic oxygen evolution in acid media. Electrochim Acta 31:1311–1316
33. Angelinetta C, Trasatti S, Atanasoska LD et al (1989) Effect of preparation on the surface and electrocatalytic properties of $RuO_2 + IrO_2$ mixed oxide electrodes. Mater Chem Phys 22:231–247
34. Jirkovský J, Makarova M, Krtil P (2006) Particle size dependence of oxygen evolution reaction on nanocrystalline RuO_2 and $Ru_{0.8}Co_{0.2}O_{2x}$. Electrochem Commun 8:1417–1422
35. Jirkovský J, Hoffmannová H, Klementová M, Krtil P (2006) Particle size dependence of the electrocatalytic activity of nanocrystalline RuO_2 electrodes. J Electrochem Soc 153: E111–E118
36. Abbott DF, Lebedev D, Waltar K et al (2016) Iridium oxide for the oxygen evolution reaction: correlation between particle size, morphology, and the surface hydroxo layer from operando XAS. Chem Mater 28:6591–6604
37. ten Kortenaar MV, Vente JF, Ijdo DJW et al (1995) Oxygen evolution and reduction on iridium oxide compounds. J Power Sources 56:51–60
38. Diaz-Morales O, Raaijman S, Kortlever R et al (2016) Iridium-based double perovskites for efficient water oxidation in acid media. Nat Commun 7:art no 12363
39. Frydendal R, Paoli EA, Knudsen BP et al (2014) Benchmarking the stability of oxygen evolution reaction catalysts: the importance of monitoring mass losses. ChemElectroChem 1:2075–2081
40. McCrory CCL, Jung S, Peters JC, Jaramillo TF (2013) Benchmarking heterogeneous electrocatalysts for the oxygen evolution reaction. J Am Chem Soc 135:16977–16987
41. Tseung ACC, Jasem S (1977) Oxygen evolution on semiconducting oxides. Electrochim Acta 22:31–34
42. Jasem SM, Tseung ACC (1979) A potentiostatic pulse study of oxygen evolution on Teflon-bonded nickel-cobalt oxide electrodes. J Electrochem Soc 126:1353–1360
43. Trasatti S (1984) Electrocatalysis in the anodic evolution of oxygen and chlorine. Electrochim Acta 29:1503–1512
44. Bockris JO, Otagawa T (1983) Mechanism of oxygen evolution on perovskites. J Phys Chem 87:2960–2971
45. Bockris JO, Otagawa T (1984) The electrocatalysis of oxygen evolution on perovskites. J Electrochem Soc 131:290–302
46. Suntivich J, May KJ, Gasteiger HA et al (2011) A perovskite oxide optimized for oxygen evolution catalysis from molecular orbital principles. Science 334:1383–1385
47. May KJ, Carlton CE, Stoerzinger KA et al (2012) Influence of oxygen evolution during water oxidation on the surface of perovskite oxide catalysts. J Phys Chem Lett 3:3264–3270
48. Kanan MW, Nocera DG (2008) In situ formation of an oxygen-evolving catalyst in neutral water containing phosphate and Co^{2+}. Science 321:1072–1075
49. Nørskov JK, Rossmeisl J, Logadottir A et al (2004) Origin of the overpotential for oxygen reduction at a fuel-cell cathode. J Phys Chem B 108:17886–17892
50. Markovic NM, Gasteiger HA, Ross PN (1997) Kinetics of oxygen reduction on Pt(hkl) electrodes: implications for the crystallite size effect with supported Pt electrocatalysts. J Electrochem Soc 144:1591
51. Maciá MD, Campiña JM, Herrero E, Feliu JM (2004) On the kinetics of oxygen reduction on platinum stepped surfaces in acidic media. J Electroanal Chem 564:141–150

52. Kuzume A, Herrero E, Feliu JM (2007) Oxygen reduction on stepped platinum surfaces in acidic media. J Electroanal Chem 599:333–343
53. Rizo R, Herrero E, Feliu JM (2013) Oxygen reduction reaction on stepped platinum surfaces in alkaline media. Phys Chem Chem Phys 15:15416–15425
54. Hoshi N, Nakamura M, Hitotsuyanagi A (2013) Active sites for the oxygen reduction reaction on the high index planes of Pt. Electrochim Acta 112:899–904
55. Van Hardeveld R, Hartog F (1969) The statistics of surface atoms and surface sites on metal crystals. Surf Sci 15:189–230
56. Romanowski W (1969) Equilibrium forms of very small metallic crystals. Surf Sci 18:373–388
57. Koper MTM (2011) Structure sensitivity and nanoscale effects in electrocatalysis. Nanoscale 3:2054–2073
58. Calle-Vallejo F, Loffreda D, Koper MTM, Sautet P (2015) Introducing structural sensitivity into adsorption–energy scaling relations by means of coordination numbers. Nature Chem 7:403–410
59. Calle-Vallejo F, Tymoczko J, Colic V et al (2015) Finding optimal surface sites on heterogeneous catalysts by counting nearest neighbors. Science 350:185–189
60. Kinoshita K (1990) Particle size effects for oxygen reduction on highly dispersed platinum in acid electrolytes. J Electrochem Soc 137:845–848
61. Tritsaris GA, Greeley J, Rossmeisl J, Nørskov JK (2011) Atomic-scale modeling of particle size effects for the oxygen reduction reaction on Pt. Catal Lett 141:909–913
62. Shinozaki K, Morimoto Y, Pivovar BS, Kocha SS (2016) Re-examination of the Pt particle size effect on the oxygen reduction reaction for ultrathin uniform Pt/C catalyst layers without influence from Nafion. Electrochim Acta 213:783–790
63. Perez-Alonso FJ, McCarthy DN, Nierhoff A et al (2012) The effect of size on the oxygen electroreduction activity of mass-selected platinum nanoparticles. Angew Chem Int Ed 51:4641–4643
64. Shao M, Peles A, Shoemaker K (2011) Electrocatalysis on platinum nanoparticles: particle size effect on oxygen reduction reaction activity. Nano Lett 11:3714–3719
65. Matsuzawa K, Fukushima T, Inaba M (2010) Shape-controlled platinum nanoparticles of different sizes and their electrochemical properties. Electrocatal 1:169–177
66. Devivaraprasad R, Ramesh R, Naresh N et al (2014) Oxygen reduction reaction and peroxide generation on shape-controlled and polycrystalline platinum nanoparticles in acidic and alkaline electrolytes. Langmuir 30:8995–9006
67. Tian N, Zhou Z-Y, Sun S-G (2008) Platinum metal catalysts of high-index surfaces: from single-crystal planes to electrochemically shape-controlled nanoparticles. J Phys Chem C 112:19801–19817
68. Huang X, Zhao Z, Fan J et al (2011) Amine-assisted synthesis of concave polyhedral platinum nanocrystals having 411 high-index facets. J Am Chem Soc 133:4718–4721
69. Wang C, Ma L, Liao L et al (2013) A unique platinum-graphene hybrid structure for high activity and durability in oxygen reduction reaction. Sci Rep 3:art no 2580
70. Devivaraprasad R, Kar T, Chakraborty A et al (2016) Reconstruction and dissolution of shape-controlled Pt nanoparticles in acidic electrolytes. Phys Chem Chem Phys 18:11220–11232
71. Li D, Wang C, Strmcnik DS et al (2014) Functional links between Pt single crystal morphology and nanoparticles with different size and shape: the oxygen reduction reaction case. Energy Environ Sci 7:4061–4069
72. Borup R, Meyers J, Pivovar B et al (2007) Scientific aspects of polymer electrolyte fuel cell durability and degradation. Chem Rev 107:3904–3951
73. Reiser CA, Bregoli L, Patterson TW et al (2005) A reverse-current decay mechanism for fuel cells. Electrochem Solid-State Lett 8:A273–A276
74. Shao-Horn Y, Sheng WC, Chen S et al (2007) Instability of supported platinum nanoparticles in low-temperature fuel cells. Top Catal 46:285–305

75. Meier JC, Galeano C, Katsounaros I et al (2012) Degradation mechanisms of Pt/C fuel cell catalysts under simulated start–stop conditions. ACS Catal 2:832–843
76. Chen S, Gasteiger HA, Hayakawa K et al (2010) Platinum-alloy cathode catalyst degradation in proton exchange membrane fuel cells: nanometer-scale compositional and morphological changes. J Electrochem Soc 157:A82–A97
77. Debe MK (2013) Tutorial on the fundamental characteristics and practical properties of nanostructured thin film (NSTF) catalysts. J Electrochem Soc 160:F522–F534
78. Debe MK, Schmoeckel AK, Vernstrom GD, Atanasoski R (2006) High voltage stability of nanostructured thin film catalysts for PEM fuel cells. J Power Sources 161:1002–1011
79. Stamenkovic V, Mun BS, Mayrhofer KJJ et al (2006) Changing the activity of electrocatalysts for oxygen reduction by tuning the surface electronic structure. Angew Chem Int Ed 45:2897–2901
80. Greeley J, Stephens IEL, Bondarenko AS et al (2009) Alloys of platinum and early transition metals as oxygen reduction electrocatalysts. Nat Chem 1:552–556
81. Jalan VM, Landsman DA (1978) Noble metal-refractory metal alloys as catalysts and method for making. US Patent 4,186,110
82. Jalan VM (1978) Noble metal/vanadium alloy catalyst and method for making. US Patent 4,202,934
83. Landsman DA, Luczak FJ (1980) Noble metal-chromium alloy catalysts and electrochemical cell. US Patent 4,316,944
84. Luczak FJ, Landsman DA (1983) Ternary fuel cell catalysts containing platinum, cobalt and chromium. US Patent 4,447,506
85. Luczak FJ, Landsman DA (1985) Ordered ternary fuel cell catalysts containing platinum and cobalt and method for making the catalysts. US Patent 4,711,829
86. Mukerjee S, Srinivasan S (1993) Enhanced electrocatalysis of oxygen reduction on platinum alloys in proton exchange membrane fuel cells. J Electroanal Chem 357:201–224
87. Mukerjee S, Srinivasan S, Soriaga MP, McBreen J (1995) Role of structural and electronic properties of Pt and Pt alloys on electrocatalysis of oxygen reduction. J Electrochem Soc 142:1409–1422
88. Toda T, Igarashi H, Uchida H, Watanabe M (1999) Enhancement of the electroreduction of oxygen on Pt alloys with Fe, Ni, and Co. J Electrochem Soc 146:3750–3756
89. Strasser P, Koh S, Anniyev T et al (2010) Lattice-strain control of the activity in dealloyed core–shell fuel cell catalysts. Nat Chem 2:454–460
90. Adzic RR, Zhang J, Sasaki K et al (2007) Platinum monolayer fuel cell electrocatalysts. Top Catal 46:249–262
91. Stamenkovic VR, Mun BS, Arenz M et al (2007) Trends in electrocatalysis on extended and nanoscale Pt-bimetallic alloy surfaces. Nat Mater 6:241–247
92. Nilekar AU, Xu Y, Zhang J et al (2007) Bimetallic and ternary alloys for improved oxygen reduction catalysis. Top Catal 46:276–284
93. Srivastava R, Mani P, Hahn N, Strasser P (2007) Efficient oxygen reduction fuel cell electrocatalysis on voltammetrically dealloyed Pt–Cu–Co nanoparticles. Angew Chem Int Ed 46:8988–8991
94. Mani P, Srivastava R, Strasser P (2011) Dealloyed binary PtM3 (M = Cu Co, Ni) and ternary PtNi3M (M = Cu Co, Fe, Cr) electrocatalysts for the oxygen reduction reaction: performance in polymer electrolyte membrane fuel cells. J Power Sources 196:666–673
95. Stamenkovic VR, Mun BS, Mayrhofer KJJ et al (2006) Effect of surface composition on electronic structure, stability, and electrocatalytic properties of Pt-transition metal alloys: Pt-skin versus Pt-skeleton surfaces. J Am Chem Soc 128:8813–8819
96. Bandarenka AS, Varela AS, Karamad M et al (2012) Design of an active site towards optimal electrocatalysis: overlayers, surface alloys and near-surface alloys of Cu/Pt(111). Angew Chem Int Ed 51:11845–11848
97. Stamenkovic VR, Fowler B, Mun BS et al (2007) Improved oxygen reduction activity on $Pt_3Ni(111)$ via increased surface site availability. Science 315:493–497

98. Zhang J, Yang H, Fang J, Zou S (2010) Synthesis and oxygen reduction activity of shape-controlled Pt_3Ni nanopolyhedra. Nano Lett 10:638–644
99. Wang D, Xin HL, Hovden R et al (2012) Structurally ordered intermetallic platinum–cobalt core–shell nanoparticles with enhanced activity and stability as oxygen reduction electrocatalysts. Nat Mater 12:81–87
100. Cui C-H, Li H-H, Liu X-J et al (2012) Surface composition and lattice ordering-controlled activity and durability of CuPt electrocatalysts for oxygen reduction reaction. ACS Catal 2:916–924
101. Jung N, Chung Y-H, Chung DY et al (2013) Chemical tuning of electrochemical properties of Pt-skin surfaces for highly active oxygen reduction reactions. Phys Chem Chem Phys 15:17079–17083
102. Li Q, Wu L, Wu G et al (2015) New approach to fully ordered fct-FePt nanoparticles for much enhanced electrocatalysis in acid. Nano Lett 15:2468–2473
103. Hodnik N, Jeyabharathi C, Meier JC et al (2014) Effect of ordering of $PtCu_3$ nanoparticle structure on the activity and stability for the oxygen reduction reaction. Phys Chem Chem Phys 16:13610–13615
104. Guo S, Zhang S, Sun S (2013) Tuning nanoparticle catalysis for the oxygen reduction reaction. Angew Chem Int Ed 52:8526–8544
105. Shao M, Chang Q, Dodelet J-P, Chenitz R (2016) Recent advances in electrocatalysts for oxygen reduction reaction. Chem Rev 116:3594–3657
106. Pickering HW (1983) Characteristic features of alloy polarization curves. Corrosion Sci 23:1107–1120
107. Erlebacher J, Aziz MJ, Karma A et al (2001) Evolution of nanoporosity in dealloying. Nature 410:450–453
108. Koh S, Strasser P (2007) Electrocatalysis on bimetallic surfaces: modifying catalytic reactivity for oxygen reduction by voltammetric surface dealloying. J Am Chem Soc 129:12624–12625
109. Strasser P (2009) Dealloyed core-shell fuel cell electrocatalysts. Rev Chem Eng 25:255–295
110. Brankovic SR, Wang JX, Adžić RR (2001) Metal monolayer deposition by replacement of metal adlayers on electrode surfaces. Surf Sci 474:L173–L179
111. Zhang J, Vukmirovic MB, Xu Y et al (2005) Controlling the catalytic activity of platinum-monolayer electrocatalysts for oxygen reduction with different substrates. Angew Chem Int Ed 44:2132–2135
112. Vukmirovic MB, Zhang J, Sasaki K et al (2007) Platinum monolayer electrocatalysts for oxygen reduction. Electrochim Acta 52:2257–2263
113. Debe MK, Steinbach AJ, Vernstrom GD et al (2011) Extraordinary oxygen reduction activity of Pt_3Ni_7. J Electrochem Soc 158:B910–B918
114. Chen C, Kang Y, Huo Z et al (2014) Highly crystalline multimetallic nanoframes with three-dimensional electrocatalytic surfaces. Science 343:1339–1343
115. Schuppert AK, Savan A, Ludwig A, Mayrhofer KJJ (2014) Potential-resolved dissolution of Pt-Cu: a thin-film material library study. Electrochim Acta 144:332–340
116. Yu Z, Zhang J, Liu Z et al (2012) Comparison between dealloyed $PtCo_3$ and $PtCu_3$ cathode catalysts for proton exchange membrane fuel cells. J Phys Chem C 116:19877–19885
117. Kelly MJ, Fafilek G, Besenhard JO et al (2005) Contaminant absorption and conductivity in polymer electrolyte membranes. J Power Sources 145:249–252
118. Malacrida P, Escudero-Escribano M, Verdaguer-Casadevall A et al (2014) Enhanced activity and stability of Pt–La and Pt–Ce alloys for oxygen electroreduction: the elucidation of the active surface phase. J Mater Chem A 2:4234–4243
119. Vej-Hansen UG, Rossmeisl J, Stephens IEL, Schiøtz J (2016) Correlation between diffusion barriers and alloying energy in binary alloys. Phys Chem Chem Phys 18:3302–3307
120. Escudero-Escribano M, Malacrida P, Hansen MH et al (2016) Tuning the activity of Pt alloy electrocatalysts by means of the lanthanide contraction. Science 352:73–76

121. Pedersen AF, Ulrikkeholm ET, Escudero-Escribano M et al (2016) Probing the nanoscale structure of the catalytically active overlayer on Pt alloys with rare earths. Nano Energy 29:249–260
122. Ulrikkeholm ET, Pedersen AF, Vej-Hansen UG et al (2016) Pt_xGd alloy formation on Pt (111): preparation and structural characterization. Surf Sci 652:114–122
123. Hernandez-Fernandez P, Masini F, McCarthy DN et al (2014) Mass-selected nanoparticles of Pt_xY as model catalysts for oxygen electroreduction. Nat Chem 6:732–738
124. Velázquez-Palenzuela A, Masini F, Pedersen AF et al (2015) The enhanced activity of mass-selected Pt_xGd nanoparticles for oxygen electroreduction. J Catal 328:297–307
125. Escudero-Escribano M, Verdaguer-Casadevall A, Malacrida P et al (2012) Pt_5Gd as a highly active and stable catalyst for oxygen electroreduction. J Am Chem Soc 134:16476–16479
126. Kondo S, Nakamura M, Maki N, Hoshi N (2009) Active sites for the oxygen reduction reaction on the low and high index planes of palladium. J Phys Chem C 113:12625–12628
127. Hara M, Linke U, Wandlowski T (2007) Preparation and electrochemical characterization of palladium single crystal electrodes in 0.1 M H_2SO_4 and $HClO_4$. Electrochim Acta 52:5733–5748
128. Chen Z, Higgins D, Yu A et al (2011) A review on non-precious metal electrocatalysts for PEM fuel cells. Energy Environ Sci 4:3167–3192
129. Zitolo A, Goellner V, Armel V et al (2015) Identification of catalytic sites for oxygen reduction in iron- and nitrogen-doped graphene materials. Nat Mater 14:937–942
130. Jasinski R (1964) A new fuel cell cathode catalyst. Nature 201:1212–1213
131. Alt H, Binder H, Sandstede G (1973) Mechanism of the electrocatalytic reduction of oxygen on metal chelates. J Catal 28:8–19
132. Jahnke H, Schönborn M, Zimmermann G (1976) Organic dyestuffs as catalysts for fuel cells. In: Schäfer FP, Gerischer H, Willig F et al (eds) Physical and chemical applications of dyestuffs. Springer, Berlin, pp 133–181
133. Bagotzky VS, Tarasevich MR, Radyushkina KA et al (1978) Electrocatalysis of the oxygen reduction process on metal chelates in acid electrolyte. J Power Sources 2:233–240
134. van Veen JAR, van Baar JF, Kroese KJ (1981) Effect of heat treatment on the performance of carbon-supported transition-metal chelates in the electrochemical reduction of oxygen. J Chem Soc Faraday Trans 77:2827–2843
135. Fuhrmann A, Wiesener K, Iliev I et al (1981) A contribution to the characterization of heat-treated electrocatalytically active tetramethoxy-phenylporphyrinato-cobalt-II. J Power Sources 6:69–81
136. Gruenig G, Wiesener K, Gamburzev S et al (1983) Investigations of catalysts from the pyrolyzates of cobalt-containing and metal-free dibenzotetraazaannulenes on active carbon for oxygen electrodes in an acid medium. J Electroanal Chem 159:155–162
137. Scherson DA, Gupta SL, Fierro C et al (1983) Cobalt tetramethoxyphenyl porphyrin—emission Mossbauer spectroscopy and O_2 reduction electrochemical studies. Electrochim Acta 28:1205–1209
138. Van Der Putten A, Elzing A, Visscher W, Barendrecht E (1986) Oxygen reduction on pyrolysed carbon-supported transition metal chelates. J Electroanal Chem 205:233–244
139. Gupta S, Tryk D, Bae I et al (1989) Heat-treated polyacrylonitrile-based catalysts for oxygen electroreduction. J Appl Electrochem 19:19–27
140. Wang H, Côté R, Faubert G et al (1999) Effect of the pre-treatment of carbon black supports on the activity of Fe-based electrocatalysts for the reduction of oxygen. J Phys Chem B 103:2042–2049
141. Lefevre M, Proietti E, Jaouen F, Dodelet J-P (2009) Iron-based catalysts with improved oxygen reduction activity in polymer electrolyte fuel cells. Science 324:71–74
142. Bashyam R, Zelenay P (2006) A class of non-precious metal composite catalysts for fuel cells. Nature 443:63–66
143. Wu G, More KL, Johnston CM, Zelenay P (2011) High-performance electrocatalysts for oxygen reduction derived from polyaniline, iron, and cobalt. Science 332:443–447

144. Zagal JH, Koper MTM (2016) Reactivity descriptors for the activity of molecular MN_4 catalysts for the oxygen reduction reaction. Angew Chem Int Ed 55:14510–14521
145. Jaouen F, Proietti E, Lefèvre M et al (2011) Recent advances in non-precious metal catalysis for oxygen-reduction reaction in polymer electrolyte fuel cells. Energy Environ Sci 4:114–130
146. Choi CH, Baldizzone C, Grote J-P et al (2015) Stability of Fe-N-C catalysts in acidic medium studied by operando spectroscopy. Angew Chem Int Ed 54:12753–12757
147. Markovic N, Ross PN (2002) Surface science studies of model fuel cell electrocatalysts. Surf Sci Rep 45:117–229
148. Trasatti S (1972) Work function, electronegativity, and electrochemical behaviour of metals. J Electroanal Chem 39:163–184
149. Conway BE, Jerkiewicz G (2000) Relation of energies and coverages of underpotential and overpotential deposited H at Pt and other metals to the "volcano curve" for cathodic H_2 evolution kinetics. Electrochim Acta 45:4075–4083
150. Auinger M, Katsounaros I, Meier JC et al (2011) Near-surface ion distribution and buffer effects during electrochemical reactions. Phys Chem Chem Phys 13:16384–16394
151. Sheng W, Gasteiger HA, Shao-Horn Y (2010) Hydrogen oxidation and evolution reaction kinetics on platinum: acid vs alkaline electrolytes. J Electrochem Soc 157:B1529–B1536
152. Seto K, Iannelli A, Love B, Lipkowski J (1987) The influence of surface crystallography on the rate of hydrogen evolution at Pt electrodes. J Electroanal Chem 226:351–360
153. Vesborg PCK, Seger B, Chorkendorff I (2015) Recent development in hydrogen evolution reaction catalysts and their practical implementation. J Phys Chem Lett 6:951–957
154. Marković NM, Sarraf ST, Gasteiger HA, Ross PN (1996) Hydrogen electrochemistry on platinum low-index single-crystal surfaces in alkaline solution. J Chem Soc Faraday Trans 92:3719–3725
155. Subbaraman R, Tripkovic D, Strmcnik D et al (2011) Enhancing hydrogen evolution activity in water splitting by tailoring Li^+-$Ni(OH)_2$-Pt interfaces. Science 334:1256–1260
156. Gong M, Wang D-Y, Chen C-C et al (2016) A mini review on nickel-based electrocatalysts for alkaline hydrogen evolution reaction. Nano Res 9:28–46
157. LeRoy RL (1979) Analysis of time-variation effects in water electrolyzers. J Electrochem Soc 126:1674–1682
158. Soares DM, Teschke O, Torriani I (1992) Hydride effect on the kinetics of the hydrogen evolution reaction on nickel cathodes in alkaline media. J Electrochem Soc 139:98–105
159. Genorio B, Strmcnik D, Subbaraman R et al (2010) Selective catalysts for the hydrogen oxidation and oxygen reduction reactions by patterning of platinum with calix[4]arene molecules. Nat Mater 9:998–1003
160. Zalitis CM, Kramer D, Kucernak AR (2013) Electrocatalytic performance of fuel cell reactions at low catalyst loading and high mass transport. Phys Chem Chem Phys 15:4329–4340
161. Zhuang Z, Giles SA, Zheng J, et al (2016) Nickel supported on nitrogen-doped carbon nanotubes as hydrogen oxidation reaction catalyst in alkaline electrolyte. Nat Commun 7:art. no. 10141